Dynamical origin of spectrally rich vocalizations in birdsong

J. D. Sitt,[1] A. Amador,[1] F. Goller,[2] and G. B. Mindlin[1]
[1]*Departamento de Física, Facultad de Ciencias Exactas y Naturales, Universidad de Buenos Aires, Ciudad Universitaria, Pabellon I (1428), Buenos Aires, Argentina*
[2]*Department of Biology, University of Utah, Salt Lake City, Utah 84112, USA*
(Received 30 April 2008; published 11 July 2008)

Birdsong is a model system for learned vocal behavior with remarkable parallels to human vocal development and sound production mechanisms. Upper vocal tract filtering plays an important role in human speech, and its importance has recently also been recognized in birdsong. However, the mechanisms of how the avian sound source might contribute to spectral richness are largely unknown. Here we show in the most widely studied songbird, the zebra finch (Taeniopygia guttata), that the broad range of upper harmonic content in different low-frequency song elements is the fingerprint of the dynamics displayed by its vocal apparatus, which can be captured by a two-dimensional dynamical model. As in human speech and singing, the varying harmonic content of birdsong is not only the result of vocal tract filtering but of a varying degree of tonality emerging from the sound source. The spectral content carries a strong signature of the intrinsic dynamics of the sound source.

DOI: 10.1103/PhysRevE.78.011905 PACS number(s): 87.19.−j, 05.45.−a, 43.80.+p

I. INTRODUCTION

Sound generation in songbirds and humans involves similar physical mechanisms [1]. Airflow passes between folds of tissue (vocal folds in humans, labia in songbirds), inducing them to vibrate [2,3]. The folds act as pneumatic valves (sound source) and modulate the pressure at the base of an upper vocal tract, which filters the sound waves before they are emitted. In this way, the source is responsible for the periodic modulation of airflow, generating a signal with a given spectral content. The filter enhances some of its frequencies and weakens others.

The hard beak and tongue of birds do not provide similar versatility for adjusting filter properties of the upper vocal tract as is available to speaking humans. In songbirds, it is thought that upper vocal tract filtering, through modulation of oropharyngeal volume and beak aperture control [4–10], serves to reduce upper harmonics to produce nearly tonal sounds. Although those studies address the origin of tonal sounds, they do not provide insight into how sounds with rich harmonic content are generated. Specifically, it is unknown to what degree variations in upper harmonic content are produced by the sound source. The source of spectral content has potentially important implications for the motor control of song production. Source generated harmonic content may emerge from the dynamics of the vibrating labia whereas upper vocal tract filtering requires active control of additional movements. Understanding the respective contributions of vocal organ and suprasyringeal vocal tract structures to harmonic richness in birdsong is therefore important for elucidating the central control mechanisms for song production and ontogeny.

Many songbirds produce nearly tonal sounds, like Canaries (Serinus canaria), Brown thrushers (Toxostoma rufum), and Cardinals (Cardinalis cardinalis). On the other hand, one of the most widely studied songbirds, the Zebra finch, alternates high-frequency tonal sounds with low-frequency vocalization which are spectrally very rich. This species breeds easily in the lab, and therefore is a widely studied animal model for vocal learning. Part of the program of research in this case focuses on unveiling the nature of its neural motor control. For this reason, it is very important to separate which features of its vocal output are directly controlled by specific neural instructions, and which emerge from the mechanics of the vocal organ. In this work, we study the vocalizations of the zebra finch from this perspective. We analyze the fundamental frequency and spectral content of the vocalizations, and show that these are strongly related. We show that this dependence can be interpreted in terms of the dynamical process involved in the onset of the valve oscillations of the syrinx. The work is organized as follows. The analysis of the experimental data is presented in Sec. II. The dynamical model, and the analysis of its solutions are discussed in Sec. III. Simulations of the theoretical model, and the acoustic synthesis of its solutions are described in Sec. IV. Section V contains our conclusions.

II. THE EXPERIMENTAL DATA

In this section we will present an acoustical description of the zebra finch song. The sounds of six zebra finches were recorded with a microphone (Audiotechnica AT 8356). We simultaneously measured the air sac pressure while the bird was spontaneously singing. The pressure recording was performed by inserting flexible cannula (Silastic laboratory tubing, 1.65 mm outer diameter) through the abdominal wall just posterior to the last rib, so that it extended a few millimeters into a thoracic air sac. The free end of the cannula was connected to a miniature piezoresistive pressure transducer (Fujikura model FPM-02PG), which was mounted on the birds back [9].

Males sing short stereotyped songs composed of different sound elements (see Fig. 1). These vary substantially in fundamental frequency (typically between 0.37–7.2 kHz). Unlike the mostly tonal songs of many other songbirds, zebra finch song elements display a wide range of spectral content

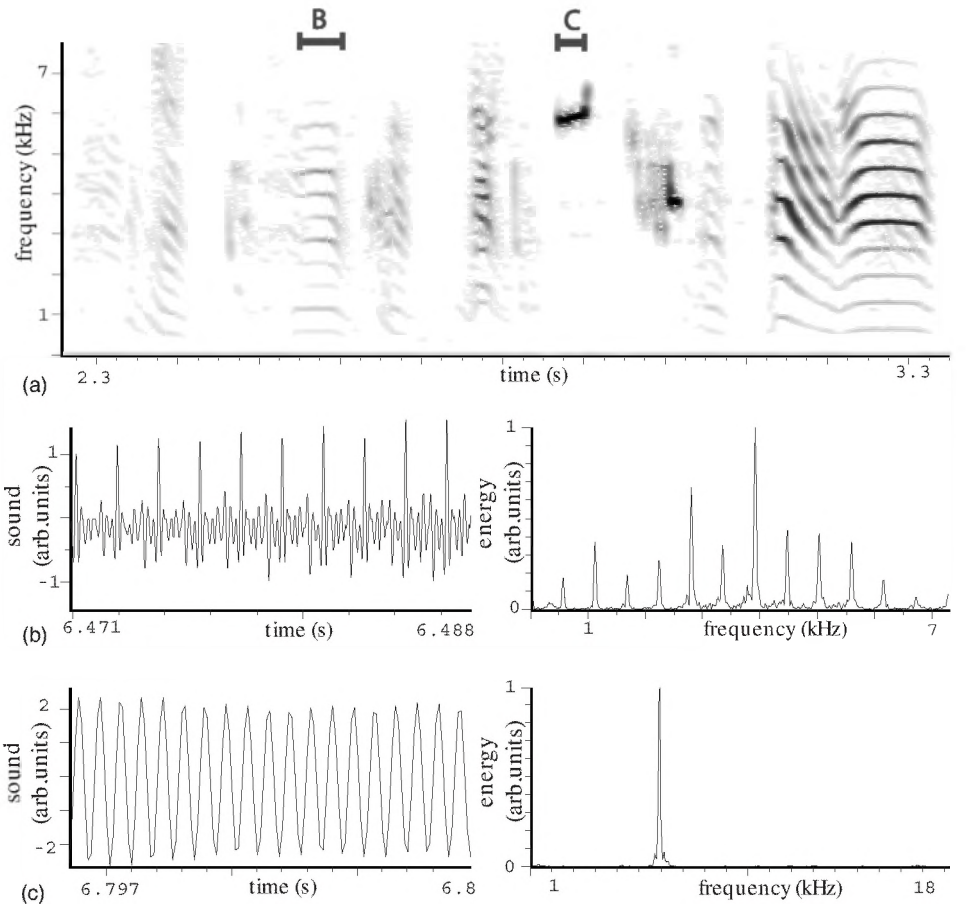

FIG. 1. Example of a zebra finch song, shown spectrographically (a). In the lower panels, examples of different sound types [indicated by the bars in (a) are analyzed: rich harmonic content sounds (B) and tonal sounds (C)]. (b). Low fundamental frequency sound wave (left panel) extracted from the bout displayed in (a), and its corresponding spectrum (right panel). (c) High fundamental frequency sound waves (left) are more sinusoidal and their spectra are less rich (right). In both right panels, the first peak corresponds to the fundamental frequency of the sound fragment: 560 Hz for (b) and 5940 Hz for (c).

from harmonic stacks to near tonal elements [as an example see Fig. 1(b) and 1(c), respectively, which are sounds waves corresponding to the syllables denoted by (b) and (c) in Figure 1(a)]. Interestingly, upper harmonic content is correlated with the fundamental frequency of sound. Low-frequency sounds (fundamental frequency below 1.5 kHz) are spectrally rich, whereas high-frequency elements are more tonal [see their corresponding spectra in the right panels of Figures 1(b) and 1(c) respectively]. In this work, we analyzed the songs of six birds and described them acoustically. This description was performed in terms of an index describing the spectral content of each syllable, and its value was compared for sounds of different average fundamental frequency.

Two parameters are obtained from the fast Fourier transform (FFT) of each sound segment: the average fundamental frequency (AFF) and the mean spectral frequency (MSF). The AFF was determined as the mean pulse rate for low-frequency sound segments and as the first peak in the FFT for high-frequency sound segments, and the MSF as the sum of the products of each frequency ω_i times the energy in that frequency ϵ_i divided by the total energy E,

$$f_{\mathrm{MSF}} = \sum_i \frac{\omega_i \epsilon_i}{E}. \tag{1}$$

The harmonic richness of a signal is usually quantified by the average energy of its spectrum. In our case, we are interested in comparing the spectral content of different syllables presenting different fundamental frequencies. In order to provide a measure of the spectral content of the syllable independently of its fundamental frequency, we define the spectral content index (SCI) as $\mathrm{SCI}=f_{\mathrm{MSF}}/f_{\mathrm{AFF}}$, which allows us to compare easily the spectral content of different syllables.

Despite being extracted from songs of different birds, in Figure 2 points with coordinates (AFF, SCI) cluster tightly within a bounded region across the (AFF, SCI) space, suggesting the existence of a simple relationship valid among a wide range of frequencies. The wide range of harmonic content present in the vocalizations, and the fact that low-frequency syllables in the zebra finch are generated by pulse-tone-like labial dynamics [11] strongly suggest that the observed systematic relationship between fundamental frequency and tonality emerges, at least in part, from the mechanism responsible for sound generation itself. To address this question, we performed a theoretical exploration of labial dynamics, in order to identify a dynamical mechanism capable of accounting for the observed relationship between spectral content and fundamental frequency. Although recently nonlinear models have shown to be consistent with a variety of complex sounds, we aim at finding a dynamical mechanism which can account for our observations in a low-dimensional model of labial dynamics.

III. A DYNAMICAL MECHANISM

In songbirds, as in humans, the generation of sound requires the onset of labial oscillations [3]. The theory of dy-

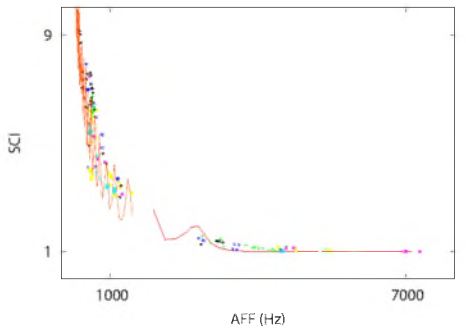

FIG. 2. (Color online) The spectral content of the syllables and sound frequency are correlated. We show the analysis for 172 sound segments uttered by six zebra finches. For each syllable we compute the spectral content index (SCI) and the average fundamental frequency (AFF) (see Methods). Each syllable analyzed is represented by a point. Different point types correspond to different birds. The dotted line is obtained through a numerical experiment where only p_s (air sac pressure), was changed generating sounds of frequency smaller than 1.5 kHz and then filtered with a tube of length 20 mm and reflection coefficient $\alpha=0.95$. The solid line was computed changing the parameters p_s (air sac pressure) and g_0 (dorsal muscle activity) from (2004 Pa, −0.04 dyn) to (2004 Pa, −0.0328 dyn) linearly and then filtered with the same tube.

namical systems allows a classification of the ways in which a physical system can undergo a qualitative change in its behavior as parameters are changed [12,13]; in our case, the ways in which a labium can abandon its stationary state for an oscillatory one. One of these ways is known in the mathematical literature as a saddle node in a limit cycle bifurcation (SNILC) [13]. The oscillatory regime starts as a stable stationary state and is annihilated by an unstable one (Fig. 3). Right after the bifurcation, the system oscillates, spending a large amount of time in the region of the phase space $(x, dx/dt)$ where the annihilation took place. The reason is that right after the bifurcation, there is a saddle node remnant. In [13] it is shown that in fact, the period T of these oscillations blows like $(a_c-a)^{-1/2}$, where a is the control parameter and a_c its value at the bifurcation point. Since close to the bifurcation, the system spends practically all the time visiting the remnant of the saddle node pair, the periodic solution looks like a sharp peak taking place during a small fraction of its period. Therefore, this mechanism provides an oscillation with a rich spectral content.

As parameters are further moved, the oscillation becomes more tonal. Therefore, this dynamical mechanism is a good candidate to account for the observed spectral features. Moreover, it can be identified in a physical model of labial dynamics.

One of the simplest physical models to account for the transfer of the kinetic energy of air flow to vocal fold oscillations is built upon experimental observation that the vocal folds support both lateral oscillations and an upward propagating surface wave [14]. As the opposing labia have a convergent profile when they move away from each other and a more planar profile when they move towards each other, there is a greater pressure on the labia during the opening phase and an overall gain in energy in each cycle of oscillation. This composed motion can be visualized as the superposition of a lateral motion and an upwards propagating wave. This model was used to synthesize sound both for humans and for birds [15,16]. We performed a mathematical implementation of this model. First, we wrote the dynamical equation for the variable x, describing the midpoint position of a labium from the rest position,

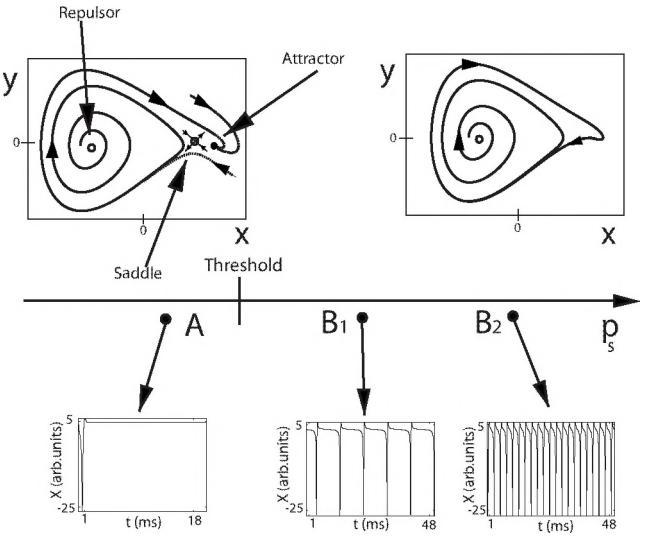

FIG. 3. The physical model can exhibit a saddle-node in a limit cycle (SNILC) bifurcation. We sketch the dynamics of the midpoint position of the labia in a region of the parameter p_s (parameter $g_0=-0.0399$ dyn), which is divided in two regions by a bifurcation line. For low values of the air sac pressure (p_s), there are three fixed points where the stationary state is stable and no oscillations occur (see A). As p_s is increased, and crosses the bifurcation line, an oscillation of zero frequency is born, with finite amplitude and a pulselike time trace (see B_1). As the pressure is further increased and the system moves away from the bifurcation line, the frequency of the solution increases, and the time trace becomes tonal (see B_2).

$$\frac{dx}{dt} = y \tag{2}$$

$$m\frac{dy}{dt} = -k(x)x - \beta(y)y - cx^2y - g_0 + a_l p_s \frac{\Delta a + 2\tau y}{a_{01} + x + \tau y}$$

$$= f(x,y), \tag{3}$$

where the first term corresponds to a nonlinear restitution force, and was approximated as $k(x)=k_1+k_2x^2$. The second term accounts for dissipation, with $\beta(y)=\beta_1+\beta_2y^2$. The third term is also a nonlinear dissipation that becomes relevant as x takes large values, corresponding to large departures from the rest position. In this way, this position dependent nonlinear dissipation serves to model collisions between labia or with containing walls, either one bounding the motion. The term g_0 is a force that is independent of the labial dynamics, and serves to model active gating [17].

Finally, the last term describes the force acting on the labium due to the interlabial pressure. It is written in terms of τ which stands for the time it takes the labial wave to propagate half the vertical size of the labia, a_l the area of the labia [14], $\Delta a=a_{01}-a_{02}$ with a_{01} and a_{02} the half separations at the

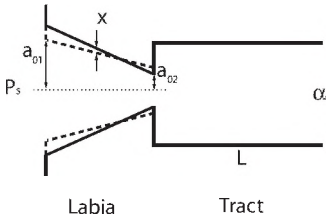

FIG. 4. Scheme of the syrinx-filter model. p_s stands for the subsiringeal pressure, x the midpoint displacement of the labia, a_{01} and a_{02} the half separations at the rest (nonoscillating) state, L the tube length, and α the reflection coefficient at the end of the trachea.

rest (nonoscillating) state [14,15] (see Fig. 4). In the last term, it was neglected the contribution due to the pressure fluctuations at the base of the tract [18]. This approximation allows a treatment of the sound oscillations independently of the properties of the filter, and leads to a paradigm known as the source-filter model for sound production. We checked numerically its applicability for the parameters of our problem.

With the numerical integration of this set of equations, we model the airflow fluctuations at the base of the vocal tract. These sound waves are filtered by the tract, which is assumed to be a tube of length L and reflection coefficient α. The pressure fluctuations at the base of the trachea at time t, $a(t)$ are given by

$$a(t) = p_f(t) - \alpha a\left(t - \frac{2L}{v}\right), \tag{4}$$

where α accounts for the reflection coefficient at the end of the trachea, p_f accounts for the pressure fluctuations induced by airflow modulations [18], and v is the sound velocity.

In this way, we model the sound in terms of a source, whose dynamics is ruled by Eqs. (2) and (3), and a filter which ultimately enhances some frequencies and depresses others. We performed a mathematical implementation of this model, and searched for a region in its parameter space where the sounds source presents the dynamical behavior described above, i.e., the arousal of oscillations with low frequency and a high spectral content.

Simulations for three different values of driving pressure within that region are illustrated in Fig. 3 (points A, B_1, and B_2). In the first case (A), the system does not oscillate. An attractor coexists with a saddle fixed point, and a repulsor. The unstable manifold of the saddle is part of the stable manifold of the attractor. In this way, when the saddle and the attractor collide in the bifurcation point, a limit cycle is created. This bifurcation is called SNILC, and is a qualitatively different process than the *Hopf* bifurcation (studied in the framework of this model in previous works [15]). The organization of the invariant manifolds described above was unveiled through numerical simulations in which a variety of initial conditions were used to generate trajectories representative of the flow. Yet, the fixed points and their local stability can be computed from Eqs. (2) and (3). They are located at $y=0$ and x such that

$$-k(x)x - g_0 + a_{ll}p_s\frac{\Delta a}{a_{01}+x} = 0. \tag{5}$$

The zeros of this function, x_f, were found numerically for the parameter values of our problem. At the bifurcation point,

$$\left.\frac{\partial f(x,y)}{\partial x}\right|_{(x_f,0)} = 0, \tag{6}$$

and therefore the Jacobian of the vector field (2) and (3) has one zero eigenvalue. For the parameters of our problem the other eigenvalue is negative. This identifies the bifurcation as a saddle node.

In the SNILC bifurcation, the oscillations preserve a signature of the slowing down that occurs in the region of the phase space where the saddle and the attractor collided. For this reason, oscillations are born not only with zero frequency but also with a high spectral richness: the oscillations differ greatly from a harmonic oscillation. Notice that as we move apart from the bifurcation point, the frequency of the oscillations increases, and the spectral content becomes poorer.

We generated synthetic data through the integration of the model for parameters fixed to, $a_{lab}=2.10^{-4}$ cm^2, $m=0.4$ ng, $k_1=0.36$ dyn/cm, $\beta_1=4.44\ 10^{-5}$ dyn s/cm, , $g_0=0.0399$ dyn, $\tau=5.10^{-6}$ s, $a_{01}=0.1$ cm, $a_{02}=0.11$ cm, $k_2=400$ dyn/cm^3 and $\beta_2=4.10^{-11}$ dyn s^3/cm^3. The spectral content was computed for 41 simulations of 114 ms (after a transient of 114 ms with a time step $dt=3.5.10^{-3}$ ms). Spectral content and fundamental frequency were analyzed in the same way as the experimental sounds. The theoretical curve (shown in Fig. 2 with a dotted line) provides a close fit to the experimental data for sounds of fundamental frequency smaller than 1.5 kHz.

This curve was generated synthesizing sounds with values of p_s from 2000 to 2008 Pa, corresponding to oscillations from 30 Hz to 1.5 kHz. The further away from the bifurcation point, the sounds had smaller periods. For each of these sounds, the spectral content was computed as in the experimental case. Later, the SCI was computed as a function of the fundamental frequency.

The tube parameters were searched so that the difference between the experimental values and their theoretical counterparts would minimized χ^2, the values found were $\alpha=0.95$ and $L=20$ mm. In Fig. 5(a), we show χ^2 as a function of α and L.

Different dynamical mechanisms would have not allowed us to recover the behavior of the SCI index along the whole range of frequencies. We tested an alternative hypothesis: that oscillations are born in a *Hopf* bifurcation instead of a SNILC, for that we used a previous minimal syrinx model [17]

$$\frac{dx}{dt} = y, \tag{7}$$

$$\frac{dy}{dt} = -k_h x - (p_s - \beta_h)y - c_h x^2 y, \tag{8}$$

in which frequency is controlled by the k_h parameter and the

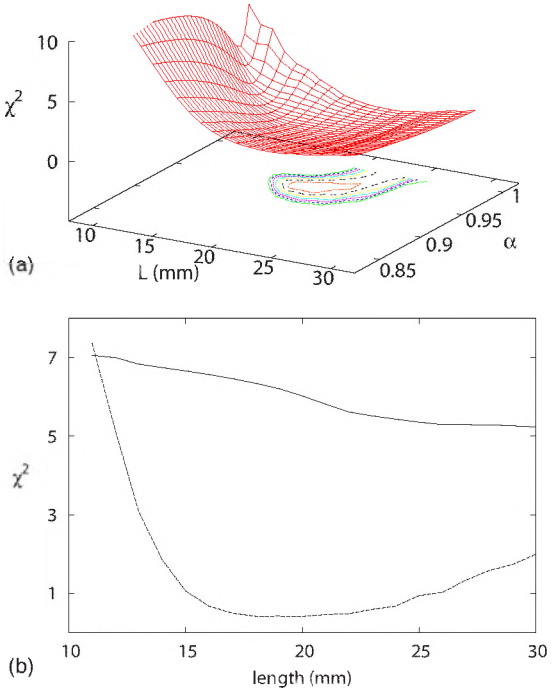

FIG. 5. (Color online) Optimization of the difference between the experimental values and their theoretical counterparts (χ^2) as a function the tube parameters of α and L. The contour is drawn at the base of the surface (a). In the lower panel we show the relationship of χ^2 and L given a fixed α=0.95 for the *Hopf* (solid line) and SNILC (dotted line) models.

Hopf bifurcation is crossed when $p_s > \beta_h$. With p_s and β_h fixed at 8000 and 1000, respectively, and sweeping k_h from 5.10^6 to 2.10^9 we generated sounds of fundamental frequencies of 350 to 7100 Hz and searched for the best filter to minimize χ^2. We found a very weak dependency of χ^2 with the filter parameters and a failure to capture the behavior of the SCI index for low frequencies. In Fig. 5(b) we show the relationship of χ^2 and L given a fixed α for the *Hopf* and SNILC models.

In this way we show that the SNILC mechanism for the onset of oscillations allows us to account for the relationship between spectral content and fundamental frequency, at least for low-frequency sounds. In this mechanism of sound production pressure alone can control the fundamental frequency of the uttered sounds. Higher frequency sounds could be synthesized further increasing the pressure, but to achieve such low spectral content, pressure should take unrealistically high values. In fact, high-frequency sounds are generated with the same values of air sac pressure used to utter low-frequency sound [see Fig. 6(a)]. Therefore air sac pressure alone can not determine the high-frequency melodies: another mechanism should be present for high frequency sounds.

In Fig. 2 we show the results of our model for high-frequency sounds. In order to synthesize these sounds, we swept the parameters g_0 and p_s from −0.04 to −0.0328 dyn and from 2004 to 2010 Pa, respectively, corresponding to oscillations from 1.5 to 6.3 kHz. This approach is consistent with experimental observations of no ventral syringeal

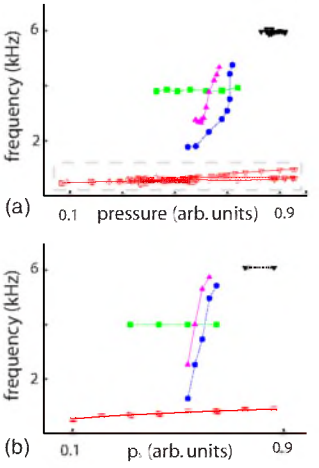

FIG. 6. (Color online) Experimental and synthetic sounds of one bird. The simultaneous measurement of sound and air sac pressure (p_s) while a zebra finch is spontaneously singing allows us to analyze the relationship between fundamental frequency of the sound and air sac pressure. Different point types correspond to different syllables. Note that in the low-frequency range [dotted rectangle in (a)] there are four different syllables. We can replicate all the different sounds with the physical model varying just p_s for low fundamental frequencies, and varying simultaneously p_s and g_0 (which represent the activity of the dorsal syringeal muscles) for high values of fundamental frequencies (b). The paths in the parameter space (p_s, g_0) to generate the synthetic syllables with high fundamental frequency are as follows: for squares from (2000.8 Pa, −0.0.384 dyn) to (2001.4 Pa, −0.0384 dyn); for down triangles from (2001.6 Pa, −0.0356 dyn) to (2000.8 Pa, −0.0356 dyn); for circles from (2001.2 Pa, −0.0399 dyn) to (2001.4 Pa, −0.0359 dyn); for up triangles from (2001.2 Pa, −0.0396 dyn) to (2001.3 Pa, −0.0359.8 dyn)

muscle activity for low-frequency sounds [19]. The data were analyzed as the low-frequency sounds for 100 simulations of 16.4 ms (after a transient of 16.4 ms with a time step $dt=2.10^{-3}$ ms), and the SCI computed for each simulation was plotted against the fundamental frequency in Fig. 2 with a continuous line.

In Fig. 6(a) we analyze the relationship between fundamental frequency of the sound and air sac pressure. Different point types correspond to different syllables. Note that in the low frequency range [dotted rectangle in Fig. 6(a)] there are four different syllables.

In the model, high-frequency sounds can be synthesized changing the parameter representing the activity of the syringeal muscles. Changing linearly the parameters representing air sac pressure and dorsal muscle activity, we generated synthetic sounds. In this way, we can achieve high fundamental frequencies with the same pressure range used for low fundamental frequencies. In Fig. 6(b), we replicate all the different sounds with the physical model varying just p_s for low fundamental frequencies, and varying simultaneously p_s and g_0 (which represent the activity of the dorsal muscles) for high values of fundamental frequencies. The paths followed in the parameter space (p_s, g_0) to generate the synthetic syllables are described in detail in caption of Fig. 6.

Low-frequency synthetic sounds were generated and filtered moving p_s close to a parameter value where a SNILC

bifurcation took place in order to generate the theoretical fit of Fig. 2 for low-frequency experimental sounds. Similarly, further changing g_0 and filtering the sound generated by the source with the same filter, we generated high-frequency sounds which fit closely the experimental points.

IV. DISCUSSION AND CONCLUSIONS

The relationship between the sound spectral content and average fundamental frequency of the different sound elements in the songs of zebra finches most likely reflects differences in source generated harmonic content, paralleling a similar relationship for the human voice [20]. Assuming that the labial oscillations responsible for the airflow modulations during the vocalizations are born in a specific dynamical way, we generated sounds with a physical model previously presented in the literature, and found a close agreement with the observed data. Although the model had been already used in the literature to emulate birdsong, it had never been explored fully in mathematical terms. For this reason, the dynamical regime presenting pulselike solutions (as the sounds uttered by zebra finches at low frequencies) had never been reported. The oscillations born in the bifurcation discussed in this article start with finite amplitude, zero frequency and pulselike shape, at a pressure threshold value. The spectral content of the sound generated depends on the pressure used during the vocalization: it becomes poorer the larger the difference between the used pressure and the threshold value. For high-frequency sounds, the use of additional motor control does not strongly affect their spectral content. Oscillations born in *Hopf* bifurcations do not show a similar dependence of spectral content on frequency, and therefore cannot account for the dynamics described here [15]. In this way, the strong dependence of spectral content on fundamental frequency emerges largely from the dynamics of the sound source in its vocal apparatus, and is less dependent on direct control of the upper vocal tract. This system illustrates the need to fully explore the deep interaction between a nervous system and the peripheral system it controls in order to understand the emerging behavior [21].

ACKNOWLEDGMENTS

This work was partially funded by UBA, CONICET, NIH, and SFI. All experimental procedures were approved by the Institutional Animal Care and Use Committee of the University of Utah.

[1] A. Doupe and P. Kuhl, Annu. Rev. Neurosci. **22**, 567 (1999).
[2] F. Goller and O. N. Larsen, Proc. Natl. Acad. Sci. U.S.A. **94**, 14787 (1997).
[3] G. B. Mindlin and R. Laje, *The Physics of Birdsong* (Springer, New York, 2005).
[4] S. Nowicki, Nature (London) **325**, 53 (1987).
[5] M. Westneat, J. J. Long, W. Hoese, and S. Nowicki, J. Exp. Biol. **182**, 147 (1993).
[6] B. Nelson, G. Beckers, and R. Suthers, J. Exp. Biol. **208**, 297 (2005).
[7] T. Riede, R. Suthers, N. Fletcher, and W. Blevins, Proc. Natl. Acad. Sci. U.S.A. **103**, 5543 (2006).
[8] R. Suthers and G. F, in *Current Ornithology*, edited by V. J. Nolan, E. Ketterson, and C. Thompson (Plenum, New York, 1997), Vol. 14, pp. 235–288.
[9] F. Goller, M. Mallinckrodt, and S. Torti, J. Neurobiol. **59**, 289 (2004).
[10] N. Fletcher, T. Riede, and R. Suthers, J. Acoust. Soc. Am. **119**, 1005 (2006).
[11] K. Jensen, B. Cooper, O. Larsen, and F. Goller, Proc. R. Soc. London, Ser. B **274**, 2703 (2007).
[12] H. Solari, M. Natiello, and GB. Mindlin, *Nonlinear Dynamics: A Two Way Trip form Physics to Math* (IOP, London, 1996).
[13] S. Strogatz, *Nonlinear Dynamics and Chaos with Applications to Physics, Biology, Chemistry, and Engineering* (Westview Press, Boulder, 2000).
[14] I. R. Titze, J. Acoust. Soc. Am. **83**, 1536 (1988).
[15] T. Gardner, G. Cecchi, M. Magnasco, R. Laje, and G. B. Mindlin, Phys. Rev. Lett. **87**, 208101 (2001).
[16] M. A. Trevisan, M. C. Eguia, and G. B. Mindlin, Phys. Rev. E **63**, 026216 (2001).
[17] R. Laje, T. Gardner, and G. B. Mindlin, Phys. Rev. E **65**, 051921 (2002).
[18] R. Laje, T. J. Gardner, and G. B. Mindlin, Phys. Rev. E **64**, 056201 (2001).
[19] D. Vicario, Neurobiology **22**, 63 (1991).
[20] I. Titze, *Principles of Voice Production* (Prentice Hall, Englewood Cliffs, 1993).
[21] H. Chiel and R. Beer, Trends Neurosci. **20**, 553 (1997).